Deciphering the morphological variation and its ontogenetic dynamics in the Late Devonian conodont Icriodus alternatus

Catherine Girard, Anne-Lise Charruault, Thomas Gluck, Carlo Corradini, Sabrina Renaud

Fossil Record @@ (@) 2022, 1–@ | DOI 10.3897/fr.@.80211

PENSOFT

MUSEUM FÜR NATURKUNDE BERLIN

Deciphering the morphological variation and its ontogenetic dynamics in the Late Devonian conodont *Icriodus alternatus*

Catherine Girard[1], Anne-Lise Charruault[1], Thomas Gluck[1], Carlo Corradini[2], Sabrina Renaud[3]

1 *Institut des Sciences de l'Evolution de Montpellier (ISEM), Univ Montpellier, CNRS, EPHE, IRD, Montpellier, France*

2 *Università degli Studi di Trieste, Dipartimento di Matematica e Geoscienze, Trieste, Italy*

3 *Laboratoire de Biométrie et Biologie Evolutive, UMR 5558, CNRS, Université Claude Bernard Lyon 1, Université de Lyon, 69622, Villeurbanne, France*

http://zoobank.org/1DC16A46-9FFC-4388-87D7-F84E2B9FD714

Corresponding author: Catherine Girard (catherine.girard@umontpellier.fr)

Academic editor: Florian Witzmann ♦ **Received** 7 January 2022 ♦ **Accepted** @ ##### 2022 ♦ **Published** @ ##### 2022

Abstract

Identification of relevant taxonomic and evolutionary units is a recurrent issue in the fossil record, and all the more for ancient fossils devoid of modern equivalents such as conodonts. Extensive morphological variation has often led to the description of numerous species, subspecies or morphotypes, which may correspond to end-member morphologies reached through ontogeny. The platform elements of the Late Devonian conodont species *Icriodus alternatus* were characterized by rows of denticles coming into occlusion between opposite elements; each element grew by the incremental addition of lamellae and by the addition of successive triads during ontogeny. During the late Frasnian and the early Famennian, the important morphological variation within this species led to the description of three subspecies. An extensive sample of early Famennian *Icriodus alternatus* was quantified using 2D biometric measurements and denticle counts on 2D pictures, showing that the subspecies mainly differed in their size range but not in their general morphology. A 3D morphometric analysis was further performed on a subsample to characterize the shape of the ontogenetically older part of the elements. During ontogeny, early valleys between denticles tended to be filled, and the asymmetry between the inner and outer side of the element increased. These ontogenetic trends are responsible for the morphologies formerly described as the subspecies *Ic. alt. mawsonae* and *Ic. alt. helmsi*. Slight discrepancies between temporal ranges of the subspecies may be achieved through variations in range of size reached by the elements as a response to environmental changes. Disparity along ontogeny seems to follow an "hourglass model" suggesting a shift from relatively loose developmental constraints to a pattern of growth modulated by functional constraints during occlusion.

Key Words

Devonian, disparity, geometric morphometrics, hourglass model, *Icriodus alternatus*

1. Introduction

Conodonts are long extinct animals known from the Cambrian to the end-Triassic, without modern equivalent. These early vertebrates were an important part of the nektonic fauna increasing in richness through the Paleozoic era (Purnell 1995). They had a well-developed feeding apparatus composed of several tooth-like elements of complex shapes. Anterior elements formed a trapping structure, whereas posterior platform elements processed food items (Aldridge et al. 1987, Purnell and Donoghue 1997). These elements functioned in occlusion between right and left elements and displayed a complex morphology, sometimes even allowing a molar-like occlusion (Donoghue and Purnell 1999). This allowed conodont animals to exploit niches of first level consumers (Balter et al. 2019). The morphological complexity of the posterior platform elements, together with their rapid temporal evolution made, them efficient stratigraphic tools for the Paleozoic and Triassic eras.

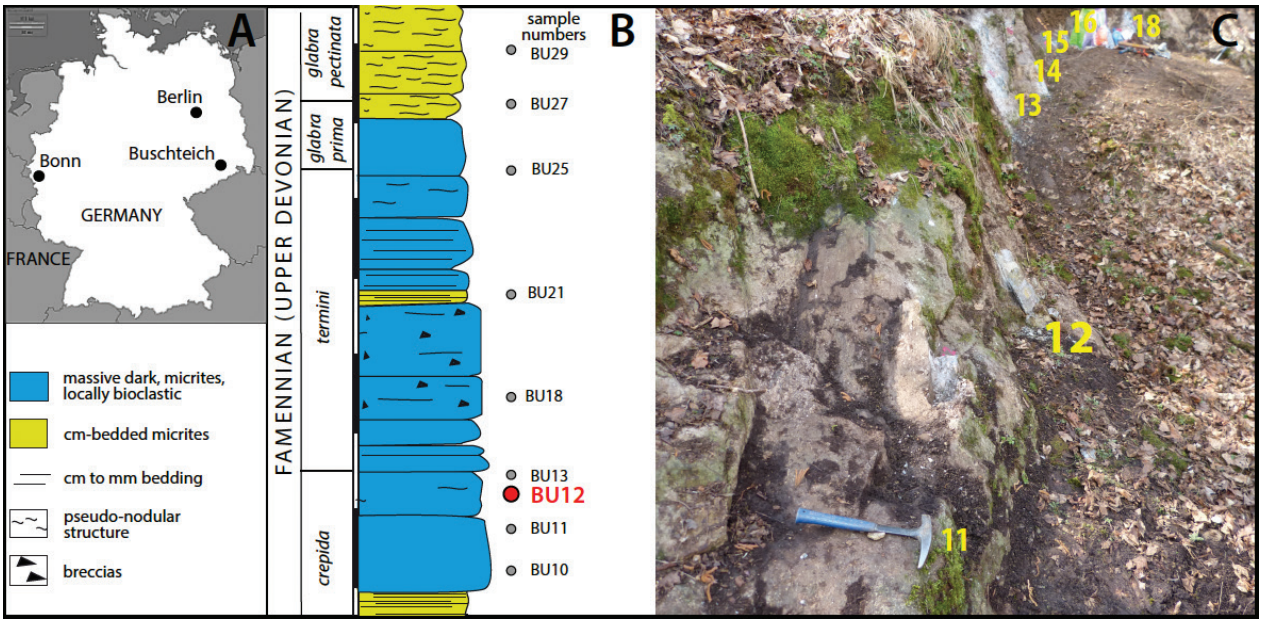

Figure 1. A. Location of the Buschteich section (Germany). **B.** Section log of the Lower Famennian in the Buschteich section and position of the studied sample, BU12 in bold (after Girard et al. 2017); **C.** Lower Famennian rocks succession in the Buschteich section.

This morphological diversity repeatedly raised the question of how to deal with an extensive phenotypic variation, leading description of numerous species, subspecies, or morphotypes (Philip and Jackson 1967, Sandberg and Ziegler 1973, Ziegler and Sandberg 1990). In the context of long extinct organisms, these concepts are not necessarily related to their meaning regarding modern animals for which genetics and behavior are crucial components to support the concept of species. As a consequence, the level to be considered as a relevant operational evolutionary unit is matter of debate (Girard et al. 2004, Girard and Renaud 2011). Conodont elements grew by the adjunction of lamellae through all the life of the animal, leading to larger elements in older animals (Donoghue 1998). Diagnostic features, and more generally, morphological variation, are also likely to increase along this continuous ontogeny, due to the fact that slight variation among individuals in the zones of preferential accretion will lead to an increasingly large phenotypic signature along growth. Considering such end-member phenotypes of a continuous variation as taxonomic units (Girard et al. 2004) might artificially inflate biodiversity estimates, and would not correspond to relevant units for evolutionary studies. Deciphering how the morphological diversity, as described by taxonomic units such as subspecies, develop along ontogeny may thus shed precious light on the operational units to be considered for evolutionary studies.

The genus *Icriodus* is documented from the Lower Devonian up to the Upper Devonian period. *Icriodus*, as many other genera, has a cosmopolitan distribution but several endemisms at specific level have been documented (Klapper and Johnson 1980, Clark 1984). Several apparatuses were described (Lange 1968, Nicoll 1982, Serpagli 1983, Simpson 1998, Suttner et al. 2017), that show a composition of twelve coniform elements and one pair of platform "Icriodontan" (I) elements. The Icriodontan elements are the characteristic feature for the description of *Icriodus* phenotypic diversity. Several species (e.g., *Ic. praealternatus*, *Ic. alternatus*, *Ic. deformatus*, *Ic. iowanensis*, *Ic. symmetricus*) have been described around the Frasnian – Famennian boundary (F/F), (numerical age 372.2; Cohen et al. 2013 updated). Despite the one of the major mass extinctions in Earth's history (McGhee 1996), pronounced temperature decrease, and sea-level fall (Joachimski and Buggisch 2002, Girard and Renaud 2007), all four species survived the crisis (Dreesen and Houllenberghs 1980, Sandberg and Dreesen 1984, Spalletta et al. 2017). Morphological diversity even led to the description of subspecies which also survived to the crisis period, questioning whether they did correspond to relevant evolutionary units. The present study aims at quantifying the morphological variation within the most abundant *Icriodus* species at that time, *Icriodus alternatus* Branson and Mehl 1934, based on material from the Buschteich section (Thuringia, Germany) (Fig. 1). The samples, include the three subspecies *Ic. alternatus alternatus*, *Ic. alt. helmsi*, and *Ic. alt. mawsonae*. These taxa were analyzed using an extensive 2D biometric analysis complemented by a 3D biometric and geometric morphometric analysis. The hypothesis to be tested was that the subspecies corresponded to end-member phenotypes of a continuous variation generated through ontogeny.

2. Presentation of *Icriodus alternatus* and taxonomic background

One natural cluster of *Icriodus alternatus* has been described (Lange 1968), but the in-vivo position and orientation of

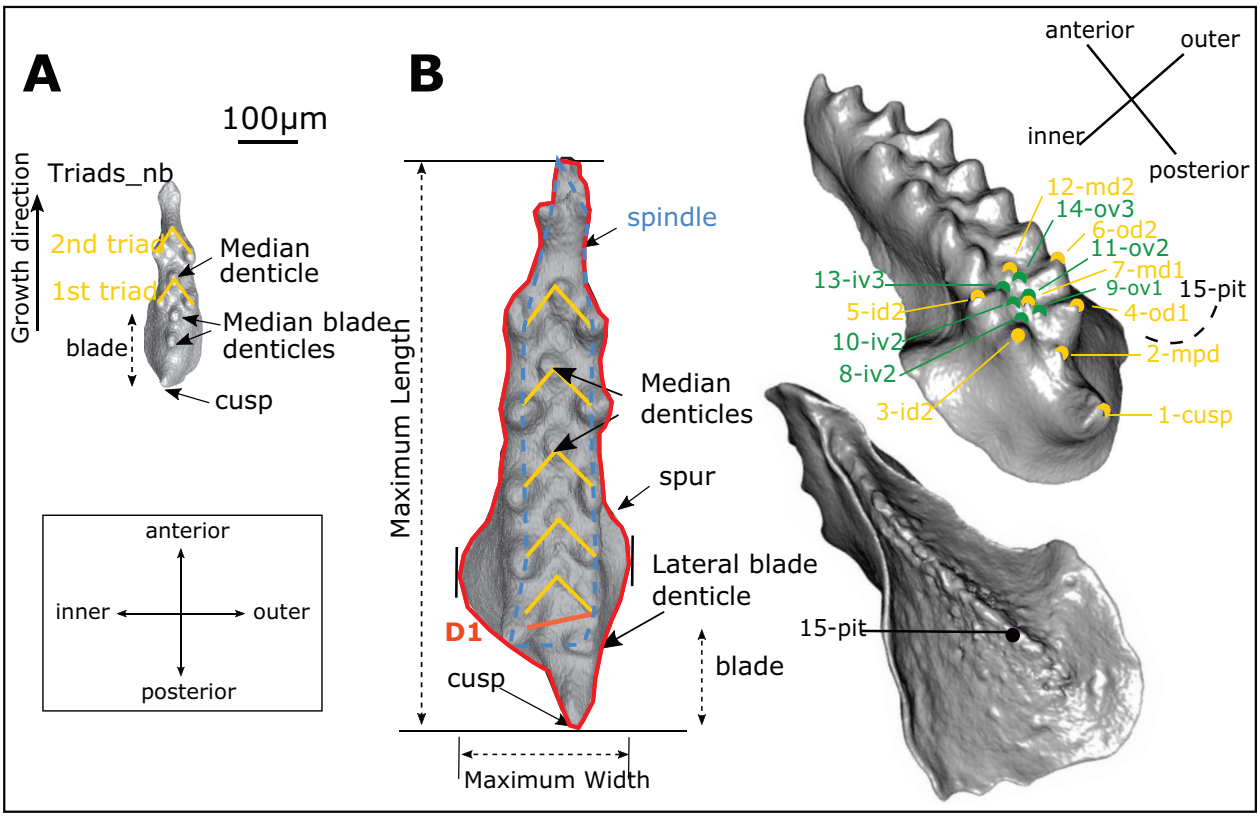

Figure 2. Morphological descriptors of I elements of *Icriodus alternatus*. **A.** "Small" specimen (UM BUS 031), upper (occlusal) view. 2D counts: Number of triads (Triads_nb): estimation of the number of triads, based on the presence of the pair of outer and inner denticles; Number of median denticles on the spindle area (Med_dent_nb); Number of lateral denticle on the blade area (Lat_blade_dent); Number of median denticle on the blade area (Med_blade_dent). **B.** *Icriodus alternatus helmsi* (UM BUS 035), upper (occlusal) view. Biometric measurements (D1, MaxLength, MaxWidth, area and spindle area). Triads in yellow; spindle area in blue dotted line, area of the 2D specimen in red, D1 distance between the inner and the outer denticles of the first triad in orange. **C.** *Icriodus alternatus alternatus* (UM BUS 033), upper and lower views (not to scale) with the position of the 3D landmarks (3D measurements). In green the valleys; in yellow the denticles.

Icriodontan elements within the animal mouth remains unknown. Therefore, the conventional nomenclature for the description of the elements ("anterior", "posterior", "inner" and "outer" side) (Branson and Mehl 1934, Sandberg and Dreesen 1984) has been retained.

The ontogenetic growth of Icriodontan elements, as described based on the species *Icriodus expansus* (Nicoll 1982), occurs through the successive addition of "triads", consisting of one median denticle and a pair of lateral denticles (Fig. 2A). The first ontogenetic stage consists of a short blade with two or three denticles and one triad. The subsequent triads are added "anteriorly", away from the blade. This ontogenetic process leads to the characteristic morphological feature of Icriodontan elements: the presence of three longitudinal rows of denticles forming a spindle (Figs 2B, 3).

Icriodus alternatus was initially characterized as bearing "denticles of the median row (…) small, rounded and isolated, alternating with the lateral denticles in position" (Branson and Mehl 1934, p. 226), with a "lachrymiform" basal cavity extending over the entire length of the element but larger in the posterior part. The authors also observed the "inconspicuousness of the median row of denticles" in *Ic. alternatus* compared to the strong denticles occurring in *Ic. symmetricus*. The reduction of the median row denticles was later emphasized by Klapper (in Ziegler 1975, p. 69), who noted that "the most distinctive aspect of the denticulation of I elements of *Ic. alternatus* is the extreme lateral compression and/or weak development of the middle row denticles. It is this feature that characterizes *Ic. alternatus*, rather than the alternation of the middle row denticles with those of the lateral rows, a denticulation common to other species of the genus".

These characteristics are highlighted in the revised diagnosis of the species (Sandberg and Dreesen 1984, p. 157). *Icriodus alternatus* was described as "A species […] in which the longitudinal axis of the I element is nearly straight and the denticles of the medial and lateral rows alternate longitudinally. The medial-row denticles are strongly reduced in height and diameter relative to the lateral-row denticles, or they are obsolescent". These authors discriminated two subspecies based on the position of the cusp, a conelike structure at the posterior extremity of the element (Fig. 2): the cusp is aligned with the median row of denticles in the nominal subspecies *alternatus*, whereas the cusp is aligned with one of the lateral rows in the sub-

species *helmsi* (Sandberg and Dreesen 1984). The authors further observed that a reduction of the median denticles, leading to a "trough" between the lateral rows of denticles, a reduction most pronounced in stratigraphically more recent specimens (Sandberg and Dreesen 1984, p. 159).

A third subspecies, *Ic. alt. mawsonae*, was later introduced by Yazdi (1999) introduced, as "a subspecies […] with a row of very weakly expressed nodes located in a central trough between lateral rows of nodes. The basal cavity follows the shape of the spindle, expanding posteriorly" (Yazdi 1999, p. 197). The author interprets the new subspecies as an "aberrant form of *Ic. alt. alternatus* with the central nodes poorly developed", and stated that *Ic. alt. mawsonae* had a "somehow larger basal" cavity than *Ic. alt. alternatus*. The characteristics of *Ic. alt. mawsonae* resemble those described by Sandberg and Dreesen (1984) for the stratigraphically late specimens of *Ic. alt. helmsi*. Indeed, the Icriodontan elements described by Yazdi (1999) come from only one sample from the upper part of an undifferentiated *crepida* Zone, that corresponds to the highest occurrence of *Ic. alt. helmsi*.

However, according to the recent revision of the Famennian conodont zonation (Spalletta et al. 2017), the three subspecies have a close stratigraphic distribution. Both *Ic. alt. alternatus* and *Ic. alt. helmsi* appeared during the Upper *rhenana* Zone (= FZ 12), whereas earliest *Ic. alt. mawsonae* are reported slightly later, during the late part of the *linguiformis* Zone (= FZ13c) (Ziegler and Sandberg 1990, Girard et al. 2005, Klapper and Kirchgasser 2016). The last occurrence (LO) of *Ic. alt. alternatus* is dated to the *Pa. gl. pectinata* (= Uppermost *crepida*) Zone, LOs of *Ic. alt. helmsi* and *Ic. alt. mawsonae* are observed slightly earlier during the *Pa. glabra prima* (= Upper *crepida*) Zone.

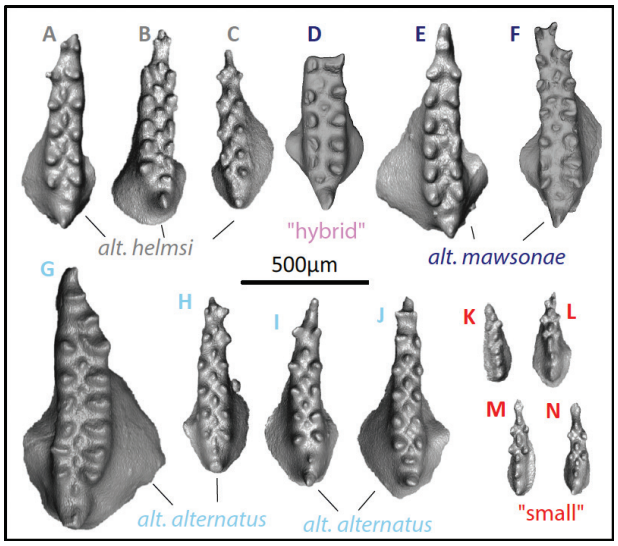

Figure 3. Morphological variation within the species *Icriodus alternatus*. Note the "hybrid" with morphological characteristic of both *helmsi* and *mawsonae*. **A.** UM BUS 034; **B.** UM BUS 035; **C.** UM BUS 036; **D.** UM BUS 037; **E.** UM BUS 038; **F.** UM BUS 039; **G.** UM BUS 033; **H.** UM BUS 040; **I.** UM BUS 041; **J.** UM BUS 042; **K.** UM BUS 043; **L.** UM BUS 044; **M.** UM BUS 045; **N.** UM BUS 031.

3. Material

The Buschteich outcrop (Thuringia, Germany), is a condensed pelagic section entirely composed of limestones (Fig. 1A, B). It contains a diverse and very abundant conodont fauna allowing the establishment of a fine biostratigraphic scheme (Girard et al. 2017). The section ranges from uppermost Frasnian to uppermost Famennian. Along this record, the present study focuses on specimens sampled from interval BU12, a level very rich in *Icriodus* elements (Girard et al. 2017), dated to the *Palmatolepis crepida* conodont Zone of Spalletta et al. (2017) (Fig. 1B, C).

Conodonts were extracted from the limestone samples following the classical procedure. Rock material was dissolved using diluted formic acid (10%). Residues were rinsed through 100 µm and 1 mm sieves; the fraction in between was dried and the conodonts were picked using a Nikon stereomicroscope. All P1 elements attributed to *Icriodus alternatus sensu lato*, hence including *Ic. alt. helmsi* and *Ic. alt. mawsonae*, were selected for the present study. Specimens with 3 triads or less were considered separate in a "small" elements group.

4. Methods

4.1. Data acquisition

4.1.1. 2D counts and measurements

A total of 191 elements were deemed to be in a suitable preservation state for a 2D quantitative study realized on SEM (Scanning Electron Microscope) pictures. Variables included the following counts (Fig. 2A):

- Number of triads (Triads_nb): estimation of the number of triads, based on the presence of the pair of outer and inner denticles;
- Number of median denticles on the spindle area (Med_dent_nb);
- Number of lateral denticle on the blade area (Lat_blade_dent);
- Number of median denticle on the blade area (Med_blade_dent).

Among these counts, the number of lateral and median denticles on the blade area were designed to characterize the *helmsi* morphotype, whereas the number of median denticles on the spindle area relative to the number of triads should characterized the *mawsonae* morphotype.

Furthermore, several 2D quantitative measurements were taken on 2D pictures of the upper (occlusal) surface of these 191 specimens using an image analysis device (Nikon NIS Elements software), in to describe the general size and shape of the elements (Fig. 2B):

- Maximum Length (MaxLength): maximum antero-posterior length of the element;

- Square root of the area of the 2D surface of the element in occlusal view (sqrtArea);
- Square root of the area of the spindle surface in occlusal view (sqrtSpinArea);
- Maximum Width (MaxWidth): largest inner-outer distance of the element;
- D1: distance between the inner and outer denticle of the first triad.

For 133 of these elements, measurements were taken on MEB pictures. A subset of 58 elements was µCT-scanned and measurements were taken on 2D snapshots of the 3D surface oriented with the occlusal surface up as for MEB pictures. The total sampling included 95 *Ic. alt. alternatus* s.s., 36 *Ic. alt. helmsi*, 17 *Ic. alt. mawsonae*, and 42 "small" specimens. One specimen displayed characters typical of both, *Ic. alt. helmsi* (most posterior denticle shifted towards the inner line of denticles) and of *Ic. alt. mawsonae* (absence of expressed first median denticle, md1) (Fig. 3D). Since the anterior was broken, it was discarded for most analyses, but was otherwise included in the *mawsonae* group.

4.1.2. Acquisition and extraction of 3D surfaces

A subset of 58 elements were glued on a toothpick and scanned at a cubic voxel resolution of ~1 µm using Phoenix Nanotom S microtomograph (µCT) on the AniRA-ImmOs platform of the SFR Biosciences, Ecole Normale Supérieure, Lyon (France). The scanning parameters were as follow: 100 kV, 70 µA, 3000 projections at 360° with no filter. The surface of the element was extracted semi-automatically using the thresholding tool in Avizo (v. 9.1—Visualization Science Group, FEI Company).

These elements were selected to document the morphological variation over a broad range of ontogenetic stages (from two to eight triads) and across subspecies. Most corresponded to *alternatus* specimens (N = 29), but the sampling included the *helmsi* (N = 11) and *mawsonae* (N = 5) subspecies. One specimen displayed characters typical of both, *helmsi*-like with the most posterior denticle shifted towards the inner row of denticles and of *mawsonae* with absence of expressed first median denticle, md1; it was depicted as "hybrid" but attributed to the subspecies *mawsonae* in statistical analyses (Fig. 3D). In the 2D analyses, "small" specimens were those with three or less triads (N = 12). Specimens with little or no damage were preferentially selected, but several broken elements were included because of their interest in documenting the morphological variation. Three specimens were anteriorly broken, hindering the measurements of their length.

All the specimens are housed in the collections of the University of Montpellier. The reconstructed 3D surfaces of the specimens illustrated on Fig. 2 and Fig. 3 (collection numbers UM BUS 031 to UM BUS 045) have been deposited in MorphoMuseuM (Girard et al. 2022).

4.1.3. Length, width and 3D landmarks

3D surfaces of the left elements, spur to the right when the element is seen in occlusal view), were subjected to a mirror transformation and measured as right elements. Length, measured as the greatest antero-posterior distance, and width, the largest inner-outer dimension, were manually measured on the 3D surfaces using Avizo. Fifteen 3D landmarks (Suppl. material 1: Table S1, Fig. 2C) were manually positioned on the surface of each element using IDAV Landmark Editor v.3.6 (Wiley et al. 2005). They document the "core" area of the element, including the blade and first two triads: being located on the first parts to develop along the ontogeny, these landmarks can be identified on all specimens including small ones. They corresponded to the tip of the cusp, the most posterior denticle (mpd) following the cusp, the tip of the inner, outer and median denticles of the first two triads, as well as the valleys between the median and lateral denticles. The pit was also documented. Defined as the deepest point of the basal cavity, its position was difficult to assess in a comparable manner in all elements, because of the occurrence of more posterior secondary "pits" in some elements. The "pit" landmark was thus taken as the deepest point in the vicinity of the first median denticle (md1).

4.2. Analysis of counts and 2D measurements

Correlations involving counts were assessed using Kendall's rank order test; correlations between numerical variables were assessed using the Pearson correlation coefficient. Differences between the *alternatus*, *helmsi*, *mawsonae*, and small groups were tested using non-parametric Kruskal-Wallis tests and pairwise Wilcoxon comparisons.

Linear models using Maximum Length as the independent variable were used to assess relationships of the different variables along ontogenetic growth, and to provide size-corrected residuals. Models including Maximum Length and group as factor were also performed. They allowed to test the significance of the differences between groups while taking size into account; the interaction between both factors indicated whether slopes were similar in the different groups.

All these tests were performed using R (R Core Team 2017).

4.3. Analyses of the 3D dataset: distances, heights, and geometric morphometrics

4.3.1. Length and width

The relationship between element length and width was assessed using a linear regression. Since width was available for all elements, the relationship length ~ width was used to interpolate length values for the three anteriorly broken specimens.

4.3.2. Characterization of the element geometry using interlandmark distances

In order to document the growth of the different parts of the elements, inter-landmark distances were calculated from the landmark coordinates. The following distances were considered:

- dlat1, distance between the inner and outer denticles of the 1st triad [= d(id1, od1)]. This distance is the equivalent in 3D of the distance D1 in 2D, but incorporates differences in height between the two lateral denticles of the triad;
- dlat2, distance between the inner and outer denticles of the 2nd triad [= d(id2, od2)]; this is the equivalent for the second triad of dlat1;
- d(cusp, mpd), distance between the cusp and the most posterior denticle following it;
- d(mpd, md1), distance from mpd to the median denticle of the 1st triad md1;
- d(mpd, id1) and d(mpd, od1), distances from mvd to the inner and outer denticles of the 1st triad, respectively.

How these distances varied along the ontogeny was investigated using linear regression of each distance *vs* element length. Interpolated values were used for visual representations but were not included in the calculation of the regressions.

4.3.3. Denticle height and pit depth: estimation by the triangle geometry

In order to estimate the height of the denticles above the valleys, geometric properties of the triangle were used. For any triangle, the semi-perimeter (p) and the area (S) can be derived can be calculated from the sides of the triangle a, b, and c, following to the two equations $p = (a + b + c) / 2$ and $S = \sqrt{p (p-a) (p-b) (p-c)}$. The altitude h at the summit A (opposed to side a) can then be obtained as $h = 2S/a$.

According to these formulas, the height of md1 can be approximated as the altitude of a triangle defined by the tip of the denticle (md1) and the two valleys surrounding it along a same line (iv1 and ov2, or alternatively ov1 and iv2) (Suppl. material 3: Fig. S1), the sides of the triangles being calculated as the corresponding inter-landmark distances. The height of md1 was thus calculated using the triangles md1-iv1-od2 and md1-od1-iv2 and assessed as the mean of both estimates. A similar procedure allowed the depth of the pit to be estimated from the same valley points.

The height of the outer and inner denticles were assessed using the valleys along the same line: h-id1, based on the triangle id1-iv1-ov2; h-od1 based on od1-ov1-iv2; h-id2 based on id2-iv2-ov1, and h-od2 based on od2-ov2-iv1.

The relationship of denticle height and pit depth with element length was assessed using linear regression. Linear models including, groups and their interaction were further investigated.

4.3.4 3D geometric morphometrics

The configurations of the fifteen 3D landmarks were superimposed using a generalized Procrustes analysis (GPA) standardizing size, position, and orientation while retaining the geometric relationships between specimens (Rohlf and Slice 1990). The aligned coordinates constituted the shape variables for further analyses. The size of the landmark configuration was estimated by the centroid size where CS: square root of the sum of squared distances from the landmarks and semi-landmarks to the centroid).

Size-related variations in shape and differences between groups (*alternatus*, *helmsi*, *mawsonae* and "small" groups were investigated using Procrustes ANOVA. With this approach, the Procrustes distances among specimens are used to quantify the components of shape variation, which are statistically evaluated via permutation, here, 9999 permutations (Adams and Otarola-Castillo 2013). The allometric relationship was visualized as the common allometric component (CAC) derived from an analysis of the aligned coordinates vs. size (Adams et al. 2013). Procrustes ANOVA were also used to assess models including size, groups, and their interaction as factors.

The Procrustes superimposition, allometric analysis, and Procrustes ANOVA were performed using the R package geomorph (Adams and Otarola-Castillo 2013).

5. Results

5.1. 2D morphological variation: overall changes with size and localized differences between subspecies

The 2D sampling included elements with two to eight triads (Fig. 4A). Maximum length increased with the number of triads (Kendall's Tau = 0.7928004, $p < 2.2e\text{-}16$). Groups were different for their maximum length (Kruskal-Wallis $p < 2.2e\text{-}16$), taken as a proxy of size. The subspecies *alternatus* covered a large size range whereas *helmsi* and *mawsonae* were both characterized by a similar large size (Fig. 4B, Table 1).

All variables, being counts or numeric measurements, were significantly related together (Fig. 5, Suppl. material 2: Table S2). Continuous measurements were particularly highly correlated with each other (e.g. Fig. 6), due to an overall increase in all dimensions when triad number increases. The distance between the inner and outer denticle of the first triad, D1, was the less strongly correlated to the other measurements. Among counts, the number of lateral denticles on the blade was the less strongly associated with other variables. One noticeable exception emerged in this pattern: the number of median denticle on the blade was significantly related with the other variables, but it decreased with triad number and overall size.

The variables specifically designed to capture the characteristics of the subspecies indeed showed significant

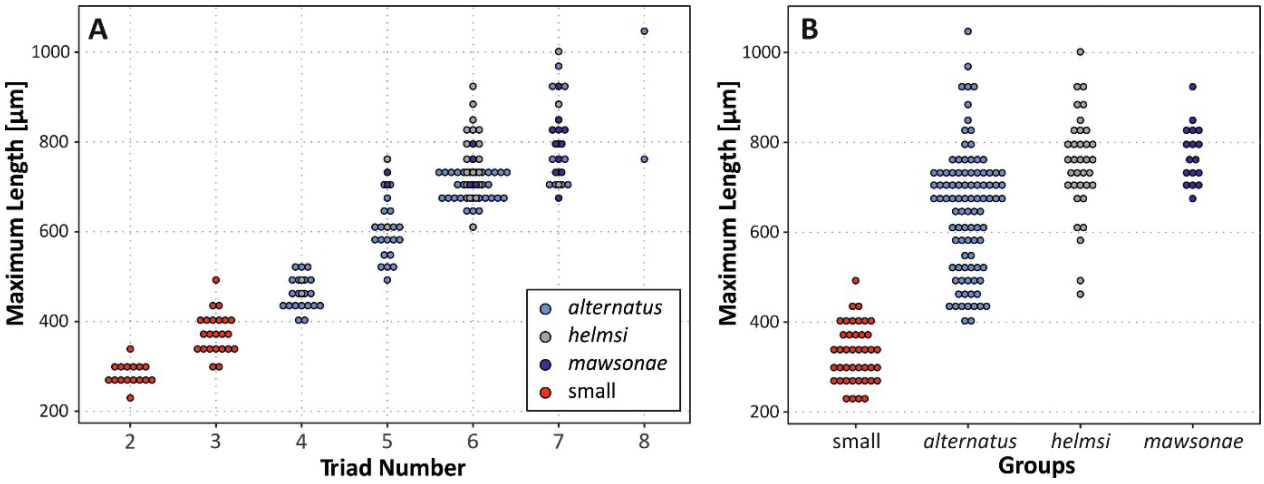

Figure 4. Maximum length of *Icriodus* elements along triad numbers (**A**) and among the subspecies (**B**) represented as dot plots. Each dot corresponds to one observation (specimen); dots within a given bin width are stacked. Here, bin width = 30.

Table 1. Differences between subspecies, for maximum length, ratio between the number of median denticles and triad number, the number of lateral denticles on the blade, and the residuals of √Area, √Spindle Area, maximum width and distance D1 vs. maximum length. KW: p-value of a Kruskal-Wallis test; if significant, p-values of pairwise Wilcoxon tests are provided below. In bold, p-value < 0.001, in italics p-value < 0.05.

Maximum Length		**KW**	**< 2.2e-16**
	small	**alternatus**	**helmsi**
alternatus	**< 2e-16**	-	-
helmsi	**< 2e-16**	**9.2e-05**	-
mawsonae	**2.9e-14**	**9.2e-05**	0.5
Med_dent_nb/Triad_nb		KW	**3.804e-06**
	small	alternatus	helmsi
alternatus	*0.0068*	-	-
helmsi	*0.0038*	0.2104	-
mawsonae	**5.2e-05**	*0.0017*	*0.0437*
Lat_Blade_Dent_nb		KW	**< 2.2e-16**
	small	alternatus	helmsi
alternatus	0.1370	-	-
helmsi	**6.9e-14**	**< 2e-16**	-
mawsonae	*0.0140*	0.106	**6.9e-06**
residuals sqrtArea		KW	0.1367
residuals sqrtSpinArea		KW	0.2194
residuals Max Width		KW	0.1759
Residuals D1		KW	0.6757

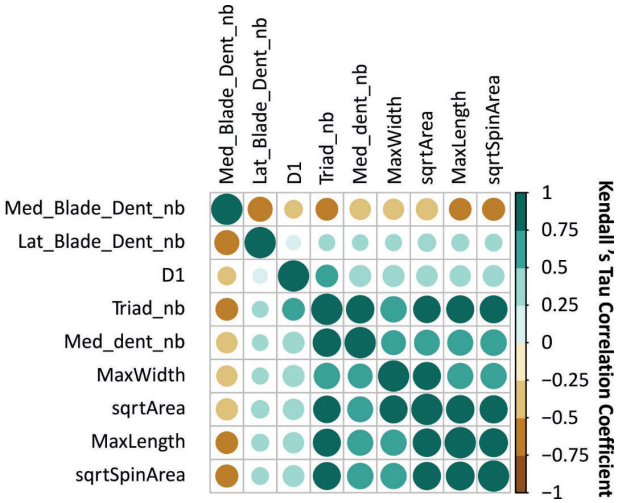

Figure 5. Correlogram of the relationship between each pair of counts and numeric variables in the *Icriodus* dataset. Size of the circle is proportional to the strength of the correlation, color varies with the value of the correlation. Kendall's tau correlation coefficient has been used for the representation. Variables are ordered according to a hierarchical clustering of the correlations.

differences. The number of median denticles on the spindle area of course increased with triad number, but to a lesser degree for *mawsonae* (Fig. 7A). As a consequence, the ratio of the median denticles number vs triad number differed between groups (Table 1).

The number of median blade denticles decreases with triad numbers (Fig. 7B), but concomitantly, the number of lateral blade denticles tends to increase, particularly in *helmsi* (Fig. 7C). As a consequence, the number of lateral blade denticles, differed between *helmsi* and the other groups (Table 1). In contrast, the subspecies did not differ in the numeric variables when the effect of size increase was taken out by considering residuals *vs.* maximum length (Table 1).

The homogeneity of the subspecies when considering their general aspect was confirmed using linear models including maximum length and groups as factors (Table 2). While maximum length always displayed a highly significant effect, the group effect was significant only for √Spindle Area and maximum width, with no significant interaction showing that the four groups shared similar slopes of variation with maximum length. However, when excluding the "small" group, the group effect was not significant anymore, showing that the three subspecies *Ic. alt. alternatus*, *Ic. alt. helmsi* and *Ic. alt. mawsonae* did not differ in their overall dimensions, when taking out the general size increase.

5.2. Disparity through ontogeny

In order to assess how morphological disparity varied along ontogeny, the variance of the different variables was assessed for each triad number. Triads 1 and 2, and

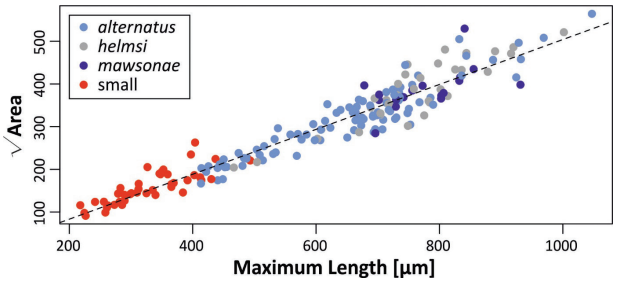

Figure 6. Relationship between maximum length and the square root of total area across the four groups of *Icriodus*. The dotted line represents the linear correlation between both variables (Pearson correlation coefficient = 0.9598, p-value < 2.2e-16).

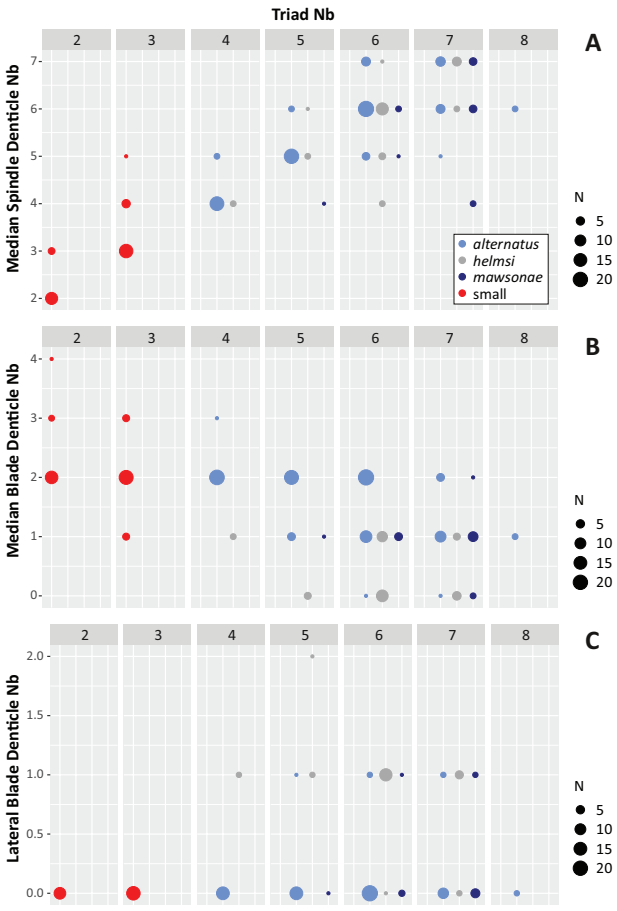

Figure 7. Number of median denticles on the spindle area (**A**), of median blade denticles (**B**) and of lateral blade denticles (**C**) along triad numbers in the four groups. The size of the symbols is proportional to the number of observations (N).

7-8, were grouped together because of insufficient data. The relative number of median denticles (Med_Dent_nb/Triads_nb) was considered together with maximum length and width, √ of the total area and spindle area, the distance between the inner and outer denticles of the first triad (D1), and the number of lateral and median denticles on the blade. To level out the effect of different scales and of size increase, variables were centered to the mean and divided by the standard deviation).

The patterns of variance through ontogeny were compared using Kendall rank order tests (Fig. 8A), showing little congruence except for maximum length,

Table 2. Effects of maximum length and subspecies (Ssp) on total area (√), spindle area (√), maximum width and the distance between the inner and outer denticle of the first triad (D1). P-values of linear models including maximum length and groups are given; left, including the four groups; right, excluding the "small" group.

	Four groups		Large only	
sqrtArea				
MaxLength	< 2e-16	***	< 2e-16	***
Ssp	0.05268		0.5478	
ML:Ssp	0.16214		0.1800	
sqrtSpinArea				
MaxLength	< 2e-16	***	< 2e-16	***
Ssp	0.03443	*	0.7423	
ML:Ssp	0.08720		0.3426	
MaxWidth				
MaxLength	< 2e-16	***	< 2e-16	***
Ssp	0.03522	*	0.9998	
ML:Ssp	0.66452		0.7563	
D1				
MaxLength	< 2e-16	***	8.632e-09	***
Ssp	0.27271		0.4680	
ML:Ssp	0.06596		0.0228	*

√Area, and √Spindle Area. However, all variables showed a minimum variance at the stage Triad 4 (Fig. 8B), to the exception of the number of lateral denticles on the blade, showing little variance in triads 1-2-3, but starting to increase in variance at triad 4. On the contrary, the variance in relative numbers of median denticles on the spindle was high in the first triads (1-2-3), decreased abruptly at triad 4, then re-increasing gently thereafter.

5.3. Variations in 3D distances and denticle heights

Length vs width in the 3D dataset

When focusing on the 3D subset, length and width measured on the 3D surfaces were strongly related (Pearson's product-moment correlation R = 0.920, p-value: < 2.2e-16), with the length increasing 1.5 faster than the length (slope of the regression: 1.509) (Suppl. material 4: Fig. S2). This regression provided interpolated length values for the three elements that have a missing anterior part.

5.4. Distances, denticle height and pit depth as a function of growth

The analysis of the heights and distances focused on the most posterior part of the element, including the first triad, because these features can be measured in almost all specimens, including small ones, and document the growth of the elements. Most variables increase with growth as indicated by increasing length (Table 3, Fig. 9). The distance between the tip of two lateral denticles of the first triad (dlat1) shows the

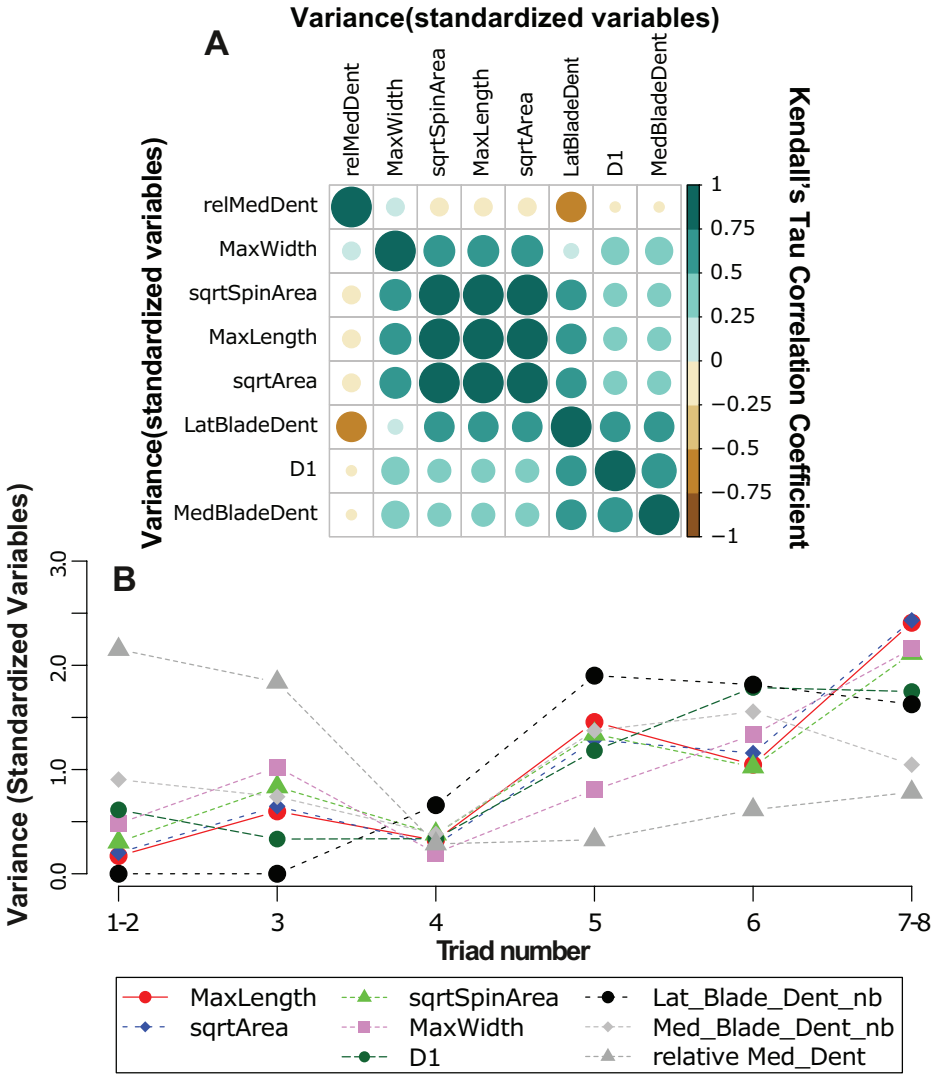

Figure 8. Disparity through ontogeny. The variance of the different reduced-centered variables was estimated for each triad number (triads 1-2 and 7-8 grouped). **A.** Correlogram showing the congruence of the pattern between variables, estimated using Kendall's tau coefficient; **B.** Change in the level of variance through ontogeny. The variance of each variable has been scaled by its mean in order to represent the different lines on a single graph. Variables considered were: MaxLength: maximum length, sqrtArea: √ of the total area of the element; sqrtSpindleArea: √ of the spindle area; MaxWidth: maximum width; D1: distance between the inner and outer denticles of the first triad; LatBladeDent: number of lateral denticles on the blade; MedBladeDent: number of median denticles on the blade; relMedDent: number of median denticles on the spindle, divided by triad number.

Table 3. Relationship of element length with inter-landmark distances, denticle height and pit depth. Above, linear model of variable vs length: R, Pearson's product-moment correlation R, associated p-value, and slope of the regression. Below, p-values of linear models with two factors: length, group [*alternatus*, *helmsi*, *mawsonae* {including the "hybrid"}, small {three or less developed triads}], and their interaction. In bold p-values < 0.001, in italics p < 0.01.

	Pit depth	Height md1	dlat1	dlat2	Height id1	Height od1	d(mpd, id1)	d(mpd, od1)	d(mpd, md1)	d(cusp, mpd)
p-value lm(~ Length)										
R	0.661	-0.639	0.896	0.797	0.434	0.599	-0.018	0.468	0.104	0.690
p-value	**4.02e-08**	**1.49e-07**	**<2.2e-16**	**3.32e-13**	**0.0009**	**1.38e-06**	0.8962	**0.0003**	0.4498	**5.70e-09**
Slope	0.06	-0.04	0.11	0.11	0.03	0.04	0.00	0.03	0.01	0.07
p-value lm(~ Length * Group)										
Length	**2.25e-08**	**1.65e-07**	**<2e-16**	**1.20e-12**	*0.0013*	**8.66e-07**	0.8968	**0.0006**	0.4298	**6.12e-09**
Group	0.0796	0.7163	0.1306	0.7346	0.4869	0.3032	0.2930	0.6098	0.1266	0.1992
*	0.2868	0.1185	0.5474	0.2235	0.8240	0.0982	0.6529	0.9989	0.1875	0.3448

tightest correlation with length, followed by the equivalent for the second triad (dlat2). The first outer denticle (od1) shows a more pronounced growth than the inner one (id1).

Three variables clearly depart from this general growth pattern. Two distances involving the most posterior denticle show no relationship with length: distance from mpd to od1 and md1. Most strikingly, the

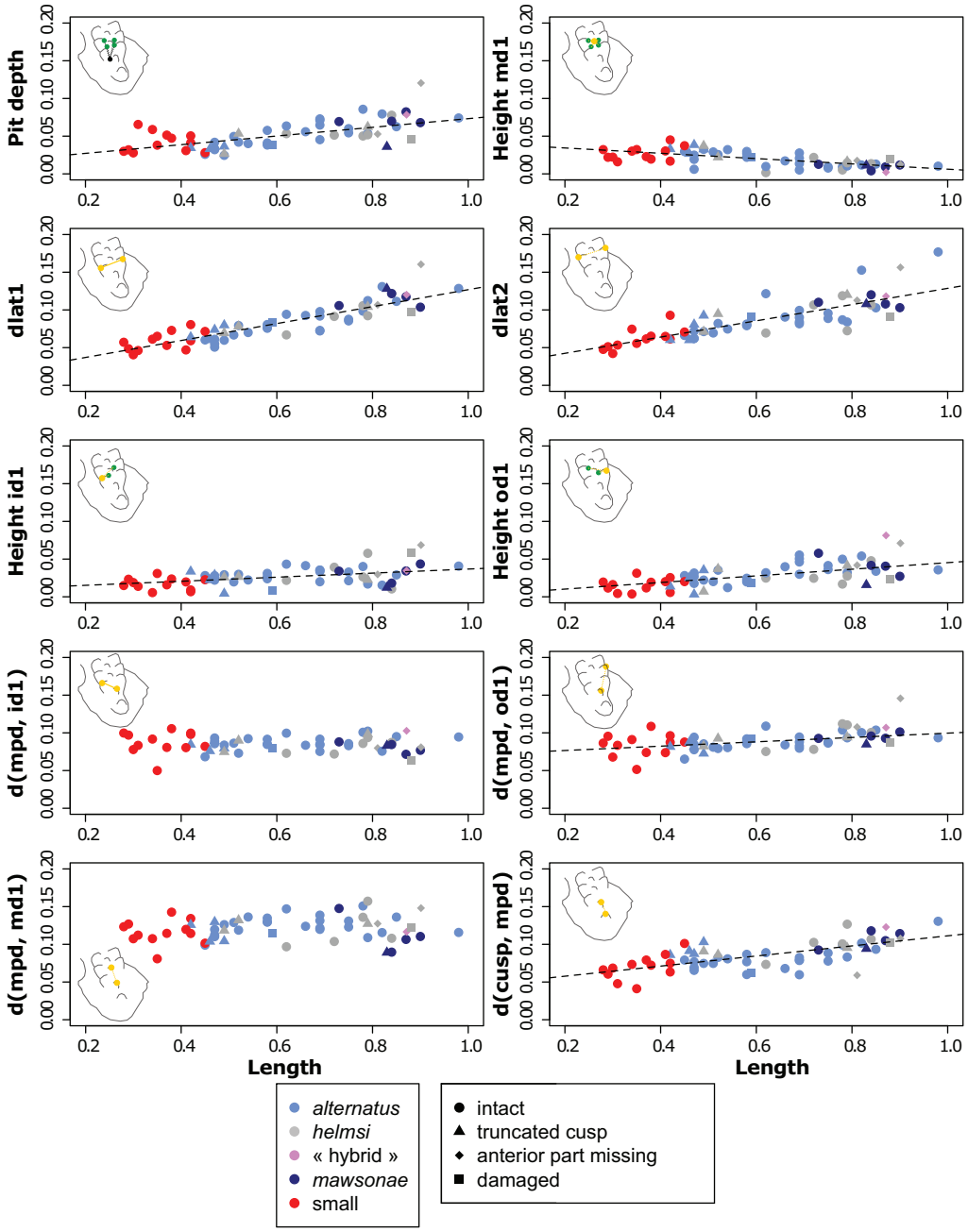

Figure 9. Relationship between Length (x-axis on all plots) and various inter-landmark distances, denticle height and pit depth. Dotted lines: significant linear relations. Interpolated values of length for the three elements with the anterior part missing (diamond symbol) are used for visualization but are not included in the regressions.

height of the first median denticle (md1) is not only stable through growth, but even decreases. Concomitantly, pit depth increases slightly faster than the height of md1. Pit depth roughly assesses the thickness of the element in the vicinity of md1, from the same valley points from which md1 height is calculated. The balance between increasing pit depth and decreasing md1 height may therefore be largely due to a filling of the valleys, ultimately leading to a md1 which is not visible anymore.

Variables can thus be associated according to the way they covary (Fig. 10). A first block of variables shows a pronounced association with length: dlat1, dlat2, pit depth, and od1 height; md1 height is also strongly associated with length, but in a negative way. The distance of the most posterior denticle (mpd) to id1 and md1 is not related to length, but is associated with other variables related to distance from mpd to the pit and to od1. The height of id1, id2 and od2 are relatively loosely related to the other variables.

These analyses were complemented by linear models including length, groups, and their interaction, in order to assess whether the growth dynamics differed between *alternatus*, *helmsi*, *mawsonae*, and the small specimens (Table 3). For all variables which were significantly related to length with a simple regression, this relation was confirmed and no difference between groups was indicated.

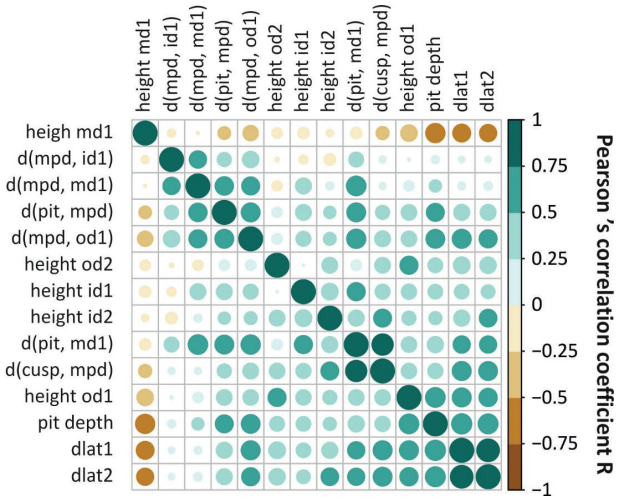

Figure 10. Correlations between univariate variables: element length (including the three interpolated values), denticle height, pit depth, and distances between denticles. In each case, the diameter of the circle and its color is proportional to the strength of the correlation, estimated using the Pearson coefficient. Variables are order to a hierarchical clustering approach.

5.5. 3D Geometric morphometrics

The Procrustes superimposition delivered the centroid size of the configurations as another proxy of element size, which was related to element length (Pearson's product-moment correlation R = 0.673, p-value = 1.811e-08) (Suppl. material 5: Fig. S3).

The morphometric analysis of the 3D shape showed along the first axis of the PCA on the aligned coordinates (PC1 = 35.2%), an opposition between small elements, towards negative scores, and *helmsi*, and especially *mawsonae*, tending to display high positive scores (Fig. 11). Scores on PC1 were highly correlated with element size (correlation with Length, including interpolated values: R = 0.891, p-value < 2.2e-16).

Therefore, the variation along PC1 mostly depicts the growth of the element. Towards negative scores corresponding to small elements, outer and inner denticles are close to and approximately at the same distance from the median axis of the element (Fig. 11B). The first median denticle is the highest, and the pit is located relatively posteriorly. Towards positive scores (Fig. 11D), in contrast, the pit is shifted towards a more anterior position. Inner and outer denticles grew in height and centrifugally from the median axis of the element; the centrifugal growth of the outer denticles being more pronounced than for the inner ones, the element acquired a torsion with an increased outer component. The most posterior denticle, maintaining its distance to the first outer and median denticles, tends to grow with an inner component. The height of the first median denticle is greatly reduced, a trend shared by the second median denticle, but to a lesser degree.

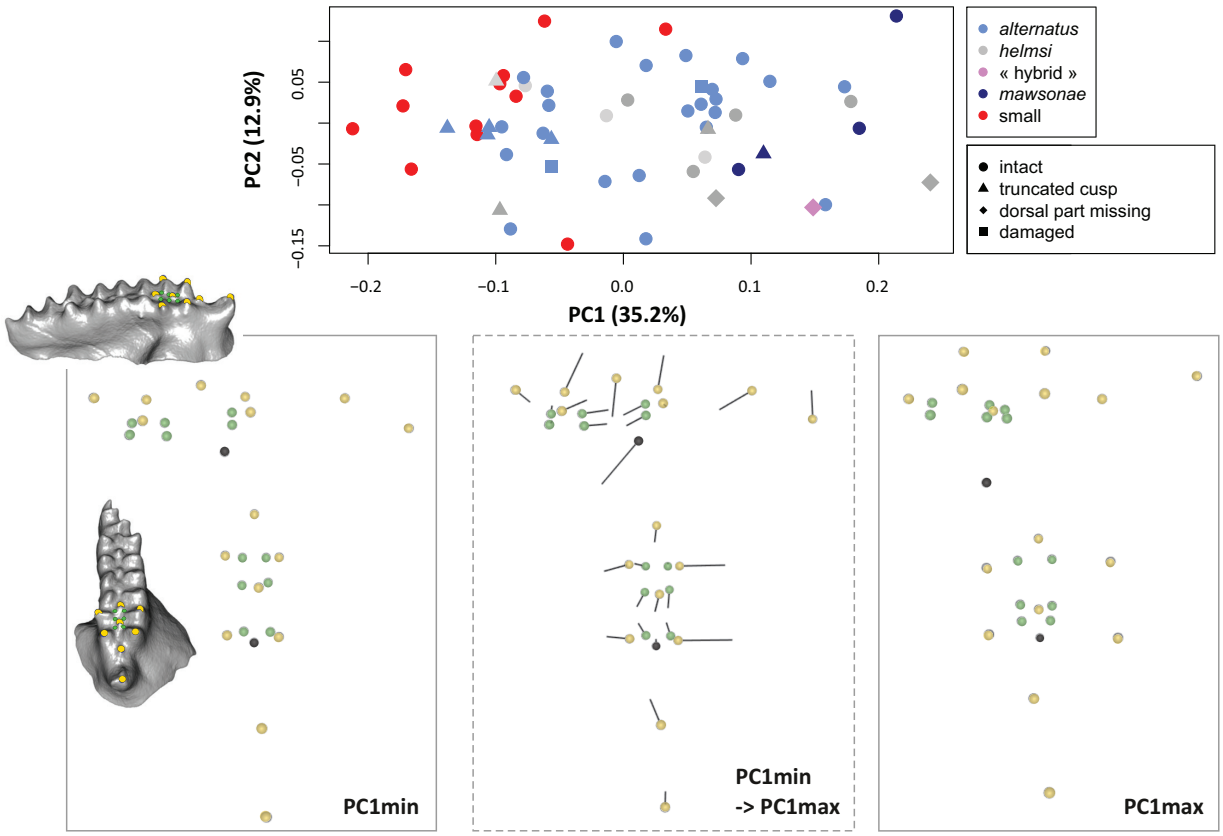

Figure 11. 3D Geometric morphometric analysis of *Icriodus alternatus* shape variation; **A.** First two axes of a PCA on the aligned coordinates; **B, C, D.** Visualization of the deformation in profile and oral view; in yellow tip of the denticles, in green valley landmarks, in black the pit; **B.** Configuration corresponding to the minimum score along PC1; **C.** Shape change from the minimum (dots) to the maximum (tip of the vectors) scores along PC1; **D.** Configuration corresponding to the maximum score along PC1.

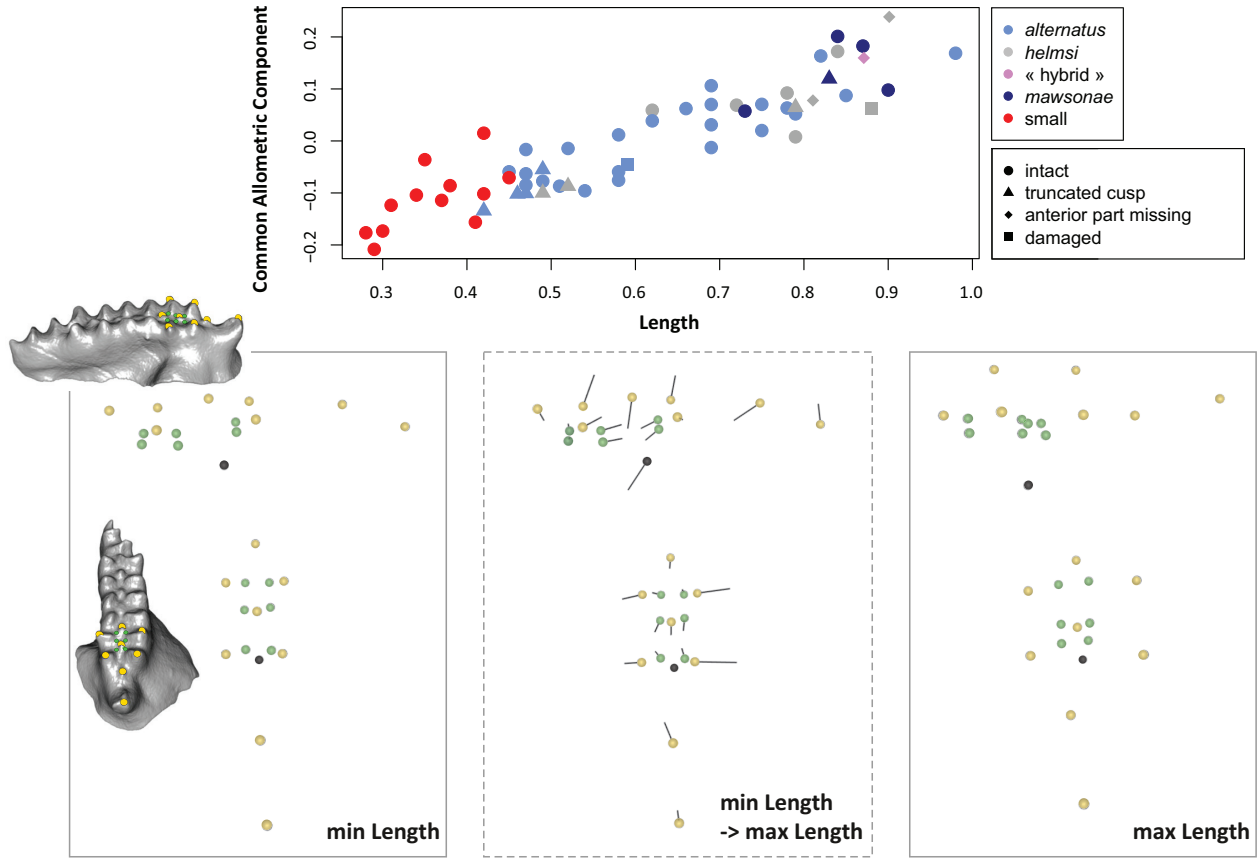

Figure 12. Allometric shape variation in *Icriodus alternatus*; **A.** Relationship between the total length of the element and the Common Allometric Component, based on the aligned coordinates of the posterior part of the element; **B, C, D.** Visualization of the deformation in profile and oral view, corresponding to extreme size values; in yellow tip of the denticles, in green valley landmarks, in black the pit; **B.** Configuration corresponding to the minimum length; **C.** Shape change from the minimum (dots) to the maximum (tip of the vectors) length; **D.** Configuration corresponding to the maximum length.

The relationship of shape with size and groups were investigated using Procrustes ANOVA. As expected, the size / shape relationship was very strong (Procrustes ANOVA, shape ~ Length including interpolated values: P = 0.0001) (Suppl. material 5: Fig. S3). When including groups as cofactors, Length remained the prominent factor, the grouping effect being close to the significance threshold (Procrustes ANOVA, shape ~ Length * Groups: $P_{Length} = 0.0001$, $P_{Groups} = 0.0627$, $P_{interaction} = 0.3435$). This difference between groups disappeared when small elements were grouped with *alternatus* ($P_{Length} = 0.0001$, $P_{Groups} = 0.3516$, $P_{interaction} = 0.3900$).

The allometric size/shape relationship can be visualized using scores along the Common Allometric Component, which highly resembles scores on PC1 (Pearson's product-moment correlation R = 0.998, p-value < 2.2e-16), underlining the importance of the allometric signal in the total shape variation. Accordingly, shape deformation associated with allometry (Fig. 12) resembles those expressed along PC1. Small specimens are characterized by shallow inner and outer denticles, organized symmetrically on both sides of the median axis of the element; the pit is shallow as well. Large elements are characterized by a deep pit, as well as elevated inner and outer denticles, the outer one being more centrifugal relative to the median axis of the element than the inner one.

6. Discussion

6.1. Subspecies describe an ontogenetic-driven morphological variation

The 3D analysis was focused on the posterior, ontogenetically oldest part of the Icriodontan element. Results showed that independently of the addition of new triads along ontogeny, the geometry of this posterior part changed deeply along growth, the main components being: (1) a growth of the inner and outer first denticles with both, a vertical and lateral component, the centrifugal growth being more pronounced for the outer denticles; (2) a growth of the cusp towards a more posterior direction, increasing its distance from the first triad; (3) a shift of the pit towards a more anterior position, together with an increase in the thickness of the element between the pit and the valleys surrounding the first median denticle; (4) a decrease in height of the first median denticle, up to its disappearance in most extreme cases. (5) In contrast, the zone comprising the most posterior denticle, the first median denticle and inner denticle, which seem to form a "core" area of the element in which the geometry, designed early during ontogeny, is little affected later on.

The subspecies *Ic. alt. alternatus*, *Ic. alt. helmsi*, and *Ic. alt. mawsonae* appeared to share the same ontogenetic trajectory, and once size-related variation is accounted for, they did not differ in any quantitative variable describing their general shape or the relationships between posterior denticles. The most prominent criterion distinguishing *Ic. alt. helmsi* and *Ic. alt. mawsonae* is their large size, suggesting that actually, these subspecies simply represent end-member geometries achieved at late growth.

The *Ic. alt. helmsi* subspecies has been characterized by the alignment of the most posterior denticle with the inner row of denticles. This morphology is achieved due to pronounced centrifugal growth of the outer denticles. Combined with the invariant relationships between the most posterior denticle and the first inner one, this trend tends to twist the shape of the large elements, up to orienting the most posterior denticle with the inner row in the most extreme cases.

As for the *Ic. alt. mawsonae* subspecies, it corresponds to an end-member of the trend of decreasing height of the first median denticles along ontogeny. Since the removal of material from a denticle seems unlikely, this decreasing height, together with the increasing thickness of the element at the vertical of the first median denticle expressed by the increase in pit depth, suggest a progressive filling of the initial deep valleys. Without a concomitant growth of the median denticle, this leads to a progressive reduction, up to its disappearance. In agreement with this interpretation of the subspecies as part of a morphological continuum including all *Ic. alternatus* subspecies, several specimens first identified as *Ic. alt. mawsonae* displayed "clear" traces of the first median denticle on the 3D scans. Furthermore, at least one specimen displayed the diagnostic features of both *Ic. alt. helmsi* and *Ic. alt. mawsonae*.

As a consequence, the described subspecies appear to belong to a single, homogeneous taxonomic and evolutionary unit, corresponding to the species *Ic. alternatus*. Although they can be seen as a way of describing an extensive morphological variation, the use of the "subspecies" concept in this context is misleading. For modern organisms, this notion corresponds to geographically isolated pools (Mayr 1963), implying some degree of gene flow breakdown. This is clearly not the case for *Ic. alt. alternatus*, *Ic. alt. helmsi* and *Ic. alt. mawsonae*, and the terminology of "subspecies" should be avoided since all can be found in the same time and place, indicating shared gene pool simply corresponding to *Icriodus alternatus*. If ever, the term "morphotype" should be preferred to describe this morphological variation, avoiding the risk to count such units in diversity analyses.

Variation in the oldest, posterior part of the element: a general feature of the genus *Icriodus*

The posterior part of the platform Icriodontan element is the first to be formed in ontogeny. As such, it is exposed to remodeling during all subsequent growth, consequently being the most variable zone in different *Icriodus* species. A morphotype differing in the expression of the denticles in the posterior area of the spindle middle row, hence similar to *Ic. alt. mawsonae*, has been described in *Icriodus subterminus* (Middle-Late Devonian) (Narkiewicz and Bultynck 2010). In another species, *Icriodus* sp. cf *Ic. brevis* (van den Boogaard 1983), the posterior denticles of the spindle, being progressively covered by new lamellae, become progressively less sharply separated from each other. The trend culminates for the three posteriormost denticles of the median row that become almost completely fused into a crest.

The blade, the other part of the element that composes the initial growth stage, displays similar trends of denticle progressive disappearance or fusion, as shown by the progressive diminution of blade denticle number along growth in *Ic. alternatus* (Dreesen and Houllenbergs 1980).

6.2. A potential for temporal changes along the ontogenetic pattern

Slight discrepancies exist in the temporal extension of the "subspecies" *Ic. alt. alternatus*, *Ic. alt. helmsi* and *Ic. alt. mawsonae*, apparently arguing for them being distinct evolutionary units. *Icriodus alternatus* as a whole appeared during a period marked by a succession of environmental perturbations. The mass extinction marking the Frasnian – Famennian boundary was the culmination of the Upper Kellwasser event materialized by anoxic deposits in many marine environments: it was associated with a pronounced temperature decrease and sea-level fall biosphere (Joachimski and Buggisch 2002, Girard and Renaud 2007). This event was preceded, *ca*. 1 myrs before, by the Lower Kellwasser event, episode of similar nature but of lesser impact on the biosphere (Joachimski and Buggisch 2002, Girard and Renaud 2007). A temperature decrease associated with a sea-level shallowing occurred towards the end of the LKE. The typical *Ic. alt. alternatus* form, together with *Ic. alt. helmsi*, appeared just after the LKE, whereas *mawsonae* appeared shortly before the UKE. Reversely, *Ic. alt. helmsi* and *Ic. alt. mawsonae* went extinct slightly before the typical *Ic. alt. alternatus* form during the early Famennian. Trends of size variation have been documented during this time period (Girard and Renaud 1996) that can explain these discrepancies. *Icriodus alternatus* displayed an increase in size in the interval between both Kellwasser events, a trend that should have promoted the apparition of *Ic. alt. mawsonae*, characterized by the largest size. Reversely, a decrease in size shortly before the species extinction might explain the disappearance of *Ic. alt. helmsi* and *Ic. alt. mawsonae* large-sized forms slightly before the final disappearance of the species. This suggests that *Icriodus alternatus* responded to environmental variations by shifts along a conserved ontogenetic trajectory, an interpretation supported by the allometric relationship between size and shape documented across the UKW and the Frasnian – Famennian crisis (Renaud and Girard 1999).

6.3. Morphological disparity along ontogeny: hint of changing constraints?

The ontogenetic pattern of *Icriodus alternatus* I elements further displayed heterogeneous disparity, with minimum morphological variance at the stage of four triads. This pattern is reminiscent of the "hourglass" developmental model (Irie and Kuratani 2014), stating that the most conserved embryonic stage is not the earliest but a mid-embryonic period called the 'phylotypic period'. This pattern has been interpreted as due to a maximum of molecular integration leading to high developmental canalization at the stage when common anatomical features of the basic body plan are defined. Regarding Icriodontan elements, this would correspond to relatively poorly constrained initial stages of development, when the earliest triads are added to the blade, converging towards the typical phenotype of the species, before that continuous growth and remodeling generate extensive morphological variation when late triads are added. Indeed, surprisingly high phenotypic variation has been found early during embryonic tooth development (Hayden et al. 2020) despite canalized adult phenotypes. Such early variation may be favored because the tooth-like structures are not yet functional. Later on, functioning may itself contribute to generate phenotypic variation in feeding structures. The morphology of Icriodontan elements suggests that the denticles were interlocked during occlusion; strong canalization would be required so that the opposite denticles would match with each other. The movement of occlusion seems to have incorporated some rotational dynamics, not only along the antero-posterior axis of the element, but also along the inner-outer axis (Suttner et al. 2017). Possibly, the addition of lamellae during late growth was influenced by the physical pressures exerted during occlusion, thus fostering the increasing asymmetry between the inner and outer denticles of the element. The "hourglass" pattern of morphological disparity along ontogeny thus suggests a shift from relatively loose developmental constraints to a pattern of growth modulated by functional constraints during occlusion. As recently suggested for the conodont genera *Polygnathus* (Renaud et al. 2021) and *Palmatolepis* (Renaud, Girard and Dufour in press), patterns of morphological variance, and not only shape itself, may be enlightening for deciphering the functional constraints related to occlusion on the platform element geometry.

7. Conclusions

2D and 3D biometric and geometric morphometric analyses have shown here that the platform (Icriodontan) elements of *Icriodus alternatus* display two major morphological trends along ontogeny, besides the addition of successive triads elongating the element: (1) a filling of the initially deep valleys between denticles on the posterior part of the element, leading to the progressive disappearance of the first median denticle on the spindle; and (2) an increasing asymmetry between the inner and outer denticles of a same triad, due to a more pronounced centrifugal growth of the outer denticle. These results suggest that the subspecies of *Icriodus alternatus* described for the end Frasnian and early Famennian constitute end-member morphologies characterizing the different growth stages. *Icriodus alternatus helmsi* and especially *Ic. alt. mawsonae* represent phenotypes achieved when large element sizes are reached, due to remodeling in relation with the continuous growth. *Icriodus alternatus alternatus* included smaller forms along the same ontogenetic trajectory. The term "subspecies" should thus be avoided to prevent the risk of artificially inflating biodiversity estimates.

Morphological disparity seems not to be homogeneous along the ontogenetic trajectory, following an "hourglass" pattern, suggesting loose developmental constraints at the beginning of the development, and increasing variance in late stages, due to continuous remodeling possibly modulated by occlusal functioning. In between, morphological variance reaches a minimum for elements with four triads. This stage may represent a "phylotypic" stage characterized by the highest canalization and hence the most discriminant between species. Taxonomic efforts should concentrate on such stages to identify relevant evolutionary relevant taxonomic units.

Data availability

Depending on the journal, the morphological data will be deposited in Dryad or as Supplementary Files. Illustrated specimens (collection numbers UM BUS 031 to UM BUS 045) are available in MorphoMuseuM.

Author contribution

CG initiated and coordinated the study. CG, ALC and CC were responsible for all aspects relevant to paleontological and geological expertise (sampling, picking, identification, dating). TG and CG acquired the 2D measurements, CG and SR analyzed the corresponding data. SR performed the 3D analyses. CG and SR wrote the first draft and all authors contributed and approved the final version of the manuscript.

Competing interest

The authors declare that they have no conflict of interest.

Acknowledgments

We acknowledge Jeff Over (Geneseo, NY) and Tomas Kumpan (Masaryck, Czech Republic) for their comments on the manuscript, and the contribution of SFR Biosciences

(UMS3444/CNRS, US8/Inserm, ENS de Lyon, UCBL) AniRa-ImmOs facility, and we particularly thank Mathilde Bouchet and Louise Souquet for their kind assistance during the scanning sessions. This work was supported by the ANR Project ECODEV (ANR-13-BSV7-005; 2014–2017) and the LabEx CeMEB project MARCON (2018–2020). This is publication ISEM 2022-003.

References

Adams CD, Otarola-Castillo E (2013) geomorph: an R package for the collection and analysis of geometric morphometric shape data. Methods in Ecology and Evolution 4: 393–399. https://doi.org/10.1111/2041-210X.12035

Aldridge RJ, Smith MP, Norby RD, Briggs DEG (1987) The architecture and function of Carboniferous polygnathacean conodont apparatus. In: Aldridge RJ (Ed.) Palaeobiology of conodonts. Ellis Horwood, Chichester, England, 63–76.

Balter V, Martin J, Tacail T, Suan G, Renaud S, Girard C (2019) Ca stable isotopes place Devonian conodonts as first level carnivores. Geochemical Perspectives Letters 10: 36–39. https://doi.org/10.7185/geochemlet.1912

Branson EB, Mehl MG (1934) Conodont studies number three. The University of Missouri studies, A quarterly of research VIII: 171–259.

Clark DL (1984) Conodont biofacies and provincialism. Geological Society of America special Paper 196, 340 pp.

Cohen KM, Finney SC, Gibbard PL, Fan J-X (2013 [updated]) The ICS International Chronostratigraphic Chart. Episodes 36: 199–204. https://doi.org/10.18814/epiiugs/2013/v36i3/002

Donoghue PCJ (1998) Growth and patterning in the conodont skeleton. Philosophical Transactions of the Royal Society London B 353: 633–666. https://doi.org/10.1098/rstb.1998.0231

Donoghue PCJ, Purnell MA (1999) Mammal-like occlusion in conodonts Paleobiology 25(1): 58–74. https://doi.org/10.1017/S0022336000031292

Dreesen R, Houllebreghs E (1980) Evolutionary trends of Famennian icriodids in the Dinant and Vestre Basins (Conodonts, Belgian Upper Devonian). Annales de la Société de Géologie de Belgique 103: 111–141.

Girard C, Charruault A-L, Gluck T, Corradini C, Renaud S (2022) 3D models related to the publication: Deciphering the morphological variation and its ontogenetic dynamics in the Late Devonian conodont *Icriodus alternatus*. MorphoMuseum. https://doi.org/10.18563/journal.m3.161

Girard C, Cornée J-J, Charruault A-L, Corradini C, Weyer D, Bartzsch K, Joachimski MM, Feist R (2017) Conodont biostratigraphy and palaeoenvironmental trends during the Famennian (Late Devonian) in the Thuringian Buschteich section (Germany), Newsletters on Stratigraphy 50(1): 71–89. https://doi.org/10.1127/nos/2016/0318

Girard C, Klapper G, Feist R (2005) Subdivision of the terminal Frasnian *linguiformis* conodont Zone, revision of the correlative interval of Montagne Noire Zone 13, and discussion of stratigraphically significant associated trilobites. In: Over DJ, Morrow JR, Wignall PB (Eds) Understanding Late Devonian and Permian-Triassic Biotic and Climatic Events: Towards an integrated approach. Devonian Palaeontological Stratigraphical Series, 181–198. https://doi.org/10.1016/S0920-5446(05)80007-X

Girard C, Renaud S (1996) Size variations in conodonts in response to the Upper Kellwasser crisis (Upper Devonian of the Montagne Noire, France). Comptes Rendus de l'Académie des Sciences, Paris 323(série IIa): 435–442.

Girard C, Renaud S (2007) Quantitative conodont-based approaches for correlation of the Late Devonian Kellwasser anoxic events. Palaeogeography Palaeoclimatology Palaeoecology 250: 114–125. https://doi.org/10.1016/j.palaeo.2007.03.007

Girard C, Renaud S (2011) The species concept in a long-extinct fossil group, the conodonts. Comptes rendus Palevol 10: 107–115. https://doi.org/10.1016/j.crpv.2010.10.009

Girard C, Renaud S, Sérayet A (2004) Morphological variation of *Palmatolepis* Devonian conodonts: species vs. genus. Comptes rendus Palevol 3: 1–8. https://doi.org/10.1016/j.crpv.2003.09.008

Hayden L, Lochovska L, Sémon M, Renaud S, Delignette-Muller M-L, Vicot M, Peterková R, Hovorakova M, Pantalacci S (2020) Developmental variability channels mouse molar evolution. eLife 9: e50103. https://doi.org/10.7554/eLife.50103

Irie N, Kuratani S (2014) The developmental hourglass model: a predictor of the basic body plan? Developmental Biology 141: 4649–4655. https://doi.org/10.1242/dev.107318

Joachimski M, Buggisch W (2002) Conodont apatite $\delta^{18}O$ signatures indicate climatic cooling as a trigger of the Late Devonian mass extinction. Geology 30(8): 711–714. https://doi.org/10.1130/0091-7613(2002)030%3C0711:CAOSIC%3E2.0.CO;2

Klapper G (1989) The Montagne Noire Frasnian (Upper Devonian) conodont succession. In: McMillan NJ, Embry AF, Glass DJ (Eds) Devonian of the World. Paleontology, Paleoecology, Biostratigraphy, Canadian Society of Petroleum Geologists, Memoir 14, Calgary, 449–468.

Klapper G, Johnson JG (1980) Endemism and dispersal of Devonian conodonts. Journal of Paleontology 54(2): 400–455. http://www.jstor.org/stable/1304071

Klapper G, Kirchgasser WT (2016) Frasnian Late Devonian conodont biostratigraphy in New York: graphic correlation and taxonomy. Journal of Paleontology 90: 525–554. https://doi.org/10.1017/jpa.2015.70

Lange FG (1968) Conodonten-Gruppenfunde aus Kalken des tieferen Oberdevon. Geologica et Palaeontologica 1: 97–114.

Mayr E (1963) Animal Species and Evolution, Mass. Belknap Press, Cambridge. https://doi.org/10.4159/harvard.9780674865327

McGhee GRJ (1996) The Late Devonian Mass Extinction – The Frasnian/Famennian crisis. Columbia University Press, New York, 303 pp.

Narkiewicz K, Bultynck P (2010) The Upper Givetian (Middle Devonian) *subterminus* conodont Zone in North America, Europe and North Africa. Journal of Paleontology 84(4): 588–625. https://doi.org/10.1666/10-029.1

Nicoll RS (1982) Multielement composition of *Icriodus expansus* Branson and Mehl from the Upper Devonian of the Canning basin, Western Australia. BMR Journal of Australian Geology and Geophysics 7: 197–213.

Philip GM, Jackson JH (1967) Lower Devonian subspecies of the conodont *Polygnathus linguiformis* Hinde from Southern Australia Journal of Paleontology 41(5): 1262–1266. http://www.jstor.org/stable/1302097

Purnell MA (1995) Microwear on conodont elements and macrophagy in the first vertebrates. Nature 374: 798–800. https://doi.org/10.1038/374798a0

Purnell MA, Donoghue PCJ (1997) Architecture and functional morphology of the skeletal apparatus of ozarkodinid conodonts. Philosophical Transactions of the Royal Society of London 352: 1545–1564. https://doi.org/10.1098/rstb.1997.0141

R Core Team (2017) R: A Language and Environment for Statistical Computing. In: R. F. f. S. Computing (Ed.) Vienna, Austria. https://www.R-project.org

Renaud S, Ecalle B, Claisse P, Charruault A-L, Ledevin R, Girard C (2021) Patterns of bilateral asymmetry and allometry in Late Devonian *Polygnathus* conodonts. Palaeontology 64(1): 137–159. https://doi.org/10.1111/pala.12513

Renaud S, Girard C (1999) Strategies of survival to extreme environmental perturbations: evolution of conodonts in response to the Kellwasser crisis (Upper Devonian). Palaeogeography Palaeoclimatology Palaeoecology 146: 19–32. https://doi.org/10.1016/S0031-0182(98)00138-2

Renaud S, Girard C, Dufour A-B (2021) Morphometric variance, evolutionary constraints and their change through time in Late Devonian *Palmatolepis* conodonts. Evolution 75–11: 2911–2929. https://doi.org/10.1111/evo.14330

Rohlf FJ, Slice D (1990) Extensions of the Procrustes method for the optimal superimposition of landmarks. Systematic Biology 39(1): 40–59. https://doi.org/10.2307/2992207

Sandberg CA, Dreesen RMJ (1984) Late Devonian icriodontid biofacies models and alternate shallow water conodont zonation. In Clark DL (Ed.) Conodont biofacies and provincialism. Geological Society of America Special Papers, Boulder/Colorado, 143–178. https://doi.org/10.1130/SPE196-p143

Sandberg CA, Ziegler W (1973) Refinement of standard Upper Devonian conodont zonation based on sections in Nevada and West Germany. Geologica et Palaeontologica 7: 97–122.

Serpagli E (1983) The conodont apparatus of *Icriodus woschmidti woschmidti*. Fossils and Strata 15: 155–161.

Simpson A (1998) Apparatus structure of the latest Silurian to Early Devonian conodont *Icriodus woschmidti hesperius* Klapper and Murphy, and some comments on phylogeny. Palaeontologica Polonica 58: 153–169. http://www.palaeontologia.pan.pl/Archive/1998-58_153-169.pdf

Spalletta C, Perri MC, Over DJ, Corradini C (2017) Famennian (Upper Devonian) conodont zonation: revised global standard. Bulletin of Geosciences 92(1): 1–27. https://doi.org/10.3140/bull.geosci.1623

Suttner TJ, Kido E, Briguglio A (2018) A new icriodontid conodont cluster with specific mesowear supports an alternative apparatus motion model for Icriodontidae. Journal of Systematic Palaeontology 16(11): 909–926. https://doi.org/10.1080/14772019.2017.1354090

van den Boogaard M (1983) Conodont faunas from Portugal and southwestern Spain. Part 7. A Frasnian conodont fauna near the Estação de Cabrela (Portugal). Scripta Geologica 69: 1–10.

Wiley DF, Amenta N, Alcantara DA, Deboshmita G, Kil YJ, Delson E, Harcourt-Smith W, Rohlf FJ, St John K, Hamann B (2005) Evolutionary morphing, VIS 05. IEEE Visualization. IEEE.

Yazdi M (1999) Late Devonian-Carboniferous conodonts from Eastern Iran. Rivista Italiana Paleontologica et Stratigraphica 105(2): 167–200.

Ziegler W (1975) Catalogue of conodonts. Vol. V. E. Schweizcrba rt'sche Verlagsbuchhandlung, 399 pp.

Ziegler W, Sandberg CA (1990) The late Devonian standard conodont zonation. Courier Forschung-Institut Senckenberg 121: 1–115.

Supplementary material 1

Table S1

Authors: Catherine Girard, Anne-Lise Charruault, Thomas Gluck, Carlo Corradini, Sabrina Renaud
Data type: table
Explanation note: Description of the 15 landmarks.

Link: https://doi.org/10.3897/fr.@.80211.suppl1

Supplementary material 2

Table S2

Authors: Catherine Girard, Anne-Lise Charruault, Thomas Gluck, Carlo Corradini, Sabrina Renaud
Data type: table
Explanation note: Correlations between variables, tested using Kendall rank order tests. Below the diagonal, Kendall's tau correlation coefficient, above the diagonal, p-value. In bold, $p < 0.001$, in italics $p < 0.05$.

Link: https://doi.org/10.3897/fr.@.80211.suppl2

Supplementary material 3

Figure S1

Authors: Catherine Girard, Anne-Lise Charruault, Thomas Gluck, Carlo Corradini, Sabrina Renaud
Data type: figure
Explanation note: Illustration of the calculation of md1 height by the geometry of the triangle iv1-md1-ov2.

Link: https://doi.org/10.3897/fr.@.80211.suppl3

Supplementary material 4

Figure S2

Authors: Catherine Girard, Anne-Lise Charruault, Thomas Gluck, Carlo Corradini, Sabrina Renaud

Data type: figure

Explanation note: Relationship between width and length of the elements. The regression (dotted line) allowed for the interpolation of the length for the three elements with their anterior part missing (pointed by arrows on the graph).

Link: https://doi.org/10.3897/fr.@.80211.suppl4

Supplementary material 5

Figure S3

Authors: Catherine Girard, Anne-Lise Charruault, Thomas Gluck, Carlo Corradini, Sabrina Renaud

Data type: figure

Explanation note: Relationship between length and geometric morphometrics of the posterior part of the element. A, Length vs Centroid Size of the posterior part. B, Length vs PC1 based on the aligned coordinates. Symbols with the thick black outline correspond to the interpolated length values.

Link: https://doi.org/10.3897/fr.@.80211.suppl5